

MOFs with 12-coordinate 5f-block metal centers

Lv, K.; Urbank, C.; Patzschke, M.; März, J.; Kaden, P.; Weiß, S.; Schmidt, M.;

Originally published:

February 2022

Journal of the American Chemical Society 144(2022)7, 2879-2884

DOI: <https://doi.org/10.1021/jacs.1c13127>

Perma-Link to Publication Repository of HZDR:

<https://www.hzdr.de/publications/Publ-34224>

Release of the secondary publication
on the basis of the German Copyright Law § 38 Section 4.

MOFs with 12-coordinate 5f-block metal centers

Kai Lv,^{†,‡,*} Christian Urbank,[‡] Michael Patzschke,[‡] Juliane März,[‡] Peter Kaden,[‡] Stephan Weiss,[‡] Moritz Schmidt^{‡,*}

[†]Radiochemistry Lab, Institute of Nuclear Physics and Chemistry (INPC), China Academy of Engineering Physics (CAEP), 621900 Mianyang, Sichuan, China

[‡]Helmholtz-Zentrum Dresden-Rossendorf (HZDR), Institute of Resource Ecology, Bautzner Landstraße 400, 01328 Dresden, Germany

KEYWORDS Actinides, 12-Coordinate, Metal-organic Frameworks, Autoluminescence, Semiconducting

ABSTRACT: We have constructed an unprecedented MOF platform that accommodates a range of 5f-block metal ions (Th⁴⁺, U⁴⁺, Np⁴⁺, Pu⁴⁺) as the primary building block. The isorecticular actinide metal-organic frameworks (An-MOFs) exhibit periodic trends in the 12-coordinate metal environment, ligand configuration, and resulting ultramicroporosity. It holds potential in distinguishing neighboring tetravalent actinides. The metal ionic radius, carboxylate bite angle, anthracene plane twisting, inter-ligand interactions, and counteraction templating collectively determine an interplay between solvation, modulation, and complexation, resulting in a coordination saturation of the central actinide while lanthanide counterparts are stabilized by the formation of a dimer-based motif. Quantum chemical calculations indicate that this large coordination number is only feasible in the high-symmetry environment provided by the An-MOFs. This category of MOFs not only demonstrates autoluminescence (4.16×10^4 counts per second per gram) but also portends a wide-bandgap (2.84 eV) semiconducting property with implications for a multitude of applications such as hard radiation detection.

The coordination number (CN) of a given metal center is essential for tuning the molecular and electronic structures, ensuing stability, and reactivity of metal complexes or coordination polymers. A low CN of metal centers will potentially offer coordinatively unsaturated metal sites for a multitude of applications¹. In contrast, the quest for large CN (i.e. > 10) remains underexplored in the realm of metal complexes or coordination polymers, wherein high CNs are originally designed by combining large actinide centers with small ligands. A CN of 15 was experimentally revealed in a thorium aminodiborane complex² while a CN of 17-24 in actinide complexes with H, He, or BH³⁻⁷ were suggested based on relativistic quantum chemical calculations. To date, the highest experimentally characterized and theoretically predicted CNs are 16 in the CoB₁₆ cluster⁸ and 28 in Ta@B₂₈³⁺ complex⁹, respectively. As these high CNs are obtained by using coordinating atoms of low-Z (i.e. H, He, B), an intriguing question is: what is the largest possible CN in molecular complexes or coordination polymers when using more common, much larger coordinating atoms such as nitrogen or oxygen? Actinide centers bearing 12 oxygen atoms have been isolated, which are mostly anionic An(NO₃)₆²⁻ ion-pair complexes^{10,11} while other complexes comprise Th⁴⁺ centers bound by two bidentate O-donor ligands and four NO₃⁻^{12,13}, or six bidentate boron oxyanions¹⁴. In one case, a thorium center is chelated by two monodentate imidazoles and five bidentate NO₃⁻, defining a unique case of the mixed-donor 12-coordinate environment¹⁵. The highest CN in MOFs is currently only 10, which is exclusively obtained with tetravalent actinides in Th-NTB¹⁶, ECUT-36¹⁷, Th-BDC-1¹⁸, SCU-11¹⁹, Th-TPO-1²⁰, Th-BTC-1²¹, SCU-8²², U4-BDC-5²³, or U4-Cl₂DHBQ²⁴. Actinide centers with a coordination number of 12 are expected

to be possible in An-MOFs that display unique structural stability, chemical reactivity, and multifunctionality²⁵, but they have not been achieved to date. Herein, we expand the CN limit to 12 in an unprecedented category of MOFs, namely An(IV)-ADC (ADC, 9,10-anthracene-dicarboxylic acid).

Four isorecticular An(IV)-ADC have been uncovered including exceedingly rare transuranium-bearing MOFs. The morphologies and defects of An(IV)-ADC crystal (e.g. Th(IV)-ADC) can be tuned by varying the precursor concentration, modulator type, and amount (Figure S1-2). In all structures, each actinide center is coordinated by six equivalent bidentate carboxylate groups from six deprotonated ADC, defining an ideal icosahedral geometry of the [AnO₁₂] primary building unit (PBU). As each ADC links two PBUs, it generates a (2,6)-connected **pcu** topology featuring a high-symmetry structure of these polyhedral crystals (Figure S3). The An-O bond length in the 12-coordinate actinide PBU follows an expected decreasing trend from 2.577 Å (Th) to 2.510 Å (Pu) due to the actinide contraction (Table 1). While the Th-O bond distance is close to the mean bond-length (i.e. 2.580 Å) of the distorted ThO₁₂ icosahedra in thorium molecular complexes, the U-O, Np-O, and Pu-O bond lengths are larger than the statistics for uranium and transuranic molecular complexes (2.518, 2.502, 2.487 Å, respectively)^{10,11,26-28}. It is notable that a subtle bond-length decrease of 0.005 Å from Np(IV) to Pu(IV), is significantly smaller than the difference in ionic radii of 0.02 Å when both have a CN of 8²⁹. Our theoretical calculations also illustrate the bond elongation, the energy of complexation (Figure S4-5), natural bond orbital (NBO) charge, d- and f-orbital occupation across (Table S1-3) from CN of 8 to CN of 12 are as expected

due to the high ionicity of metal-ligand interactions, implying that the observed CN of 12 partly results from the high-symmetry crystal structure and would not be possible with free ligands. The bite angle (θ_1) - i.e. the O-An-O bond angle - corresponds to the space that bidentate carboxylate groups take up in the coordination sphere of a central metal and depends on repulsion between interdonor atoms. An increasing trend in θ_1 can then be ascribed to enhanced ionic interaction between the actinide center with the bidentate carboxylates. These values are larger than those of nitrate in $(\text{NH}_4)_2\text{An}(\text{NO}_3)_6$ (An = Th^{4+} , Pu^{4+})¹⁰, indicating relatively stronger interdonor repulsion between the coordinating ADC in the PBU. This elevated repulsion across the actinides also contributes to an increase in the twisting angle (θ_2) of carboxylate groups relative to their anthracene planes. Every four anthracene planes along three crystallographic axes assemble into a truncated cube-like cavity, where specific dihedral angles for opposite “seesaw-like” anthracene planes (θ_3 , θ_4) define rectangular ultramicroporous “gates” (Figure S6). A subtle change of pore size and solvent-accessible void can be observed as a function of ionic radius and bite angle. Although ~50% of the framework void is determined to be accessible, the analysis of the experimental CO_2 adsorption data yields a BET surface area of 33.7 m^2/g and an approximate median pore diameter of 5.8 Å (Figure S7). Compared with other pore textures in An-MOFs²⁵, the accessible ultramicropore regime in An(IV)-ADC is relatively small and its potential in adsorption-related applications will need to be investigated in more detail.

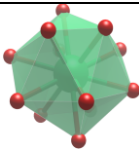
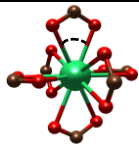
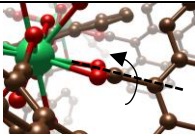
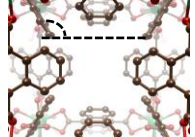
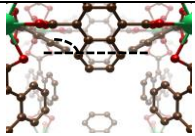
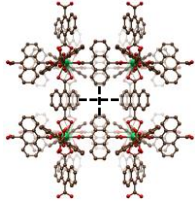
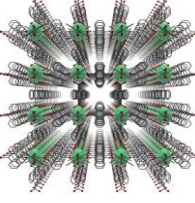
The crystallographically disordered DMF molecules and dimethylamine cations are assigned in the void, thus defining a general chemical formula as $\text{An}(\text{ADC})_3 \cdot (\text{DMF})_3 \cdot ((\text{CH}_3)_2\text{NH}_2)_2$ (Table S4). The mass loss below 200 °C, determined for Th(IV)-ADC by TGA, is assigned to the evaporation of DMF followed by the decomposition of ligands and conversion to ThO_2 (Figure S8). It is thermally stable up to about 210 °C, close to that of Pu-UiO-66 with both missing linkers and clusters defects³⁰. This low thermal stability appears to be related to fissure-like crystal defects (Figure S9) as evidenced by increasing poor integration statistics (Table S6) compared to as-synthesized material. Its structure remains intact after immersing in 0.01 $\text{mol}\cdot\text{L}^{-1}$ HNO_3 and H_2O for 5 days (Figure S10). A residual crystallinity and considerable thorium leaching rate imply that it partially degrades in 8 $\text{mol}\cdot\text{L}^{-1}$ HNO_3 while a few 12-coordinate thorium centers retain within the framework. In terms of self-irradiation stability, a variation of the unit cell length by approximately 0.08%, and 0.02% was observed for Th(IV)-U(IV)-ADC and Np(IV)-ADC, respectively, while a shrinkage of the unit cell by approximately 0.6% and “crystalline-to-amorphous” pattern in U(IV)-ADC indicates the formation of missing-metal or missing-linker defects concomitant with the formation of an unknown molecular species, leading to a change in the crystal color from blackish green to dark red (Figure S11). This self-irradiation damage is unsurprising in coordination polymers containing high-activity actinides^{31,32}. The notable structure lifetime and tiny structure change manifest the stability of 12-coordinate transuranic MOFs. The tolerance of these An-MOFs towards chemical or radiation damage is a result of the large coordination number and the ability to compensate defects with either solvent or modulator molecules.

The large ionic radii of Ln(III, IV) and U(III) are also expected to be able to form such 12-coordinate PBU in MOFs consider-

ing the presence of 12-coordinate homoleptic Ln dicyanonitrosomethanide (Ln = La-Nd, Sm) ionic liquids³³, or heteroleptic lanthanum phenanthroline-diamide complexes³⁴. However, it turns out that Ln(III, IV) assemble into 8-, or 9-coordinate Ln-ADC dimer (Figure S12) while U(III) forms a framework (Figure S13a, Figure S16) near-identical to U(IV)-ADC, implying that a majority of U(III) is in situ oxidized to U(IV) likely due to the high reactivity of U(III)³⁵. Further identification of the oxidation kinetics of U(III) precursor would be needed to pinpoint the synthetic variables that would lead to the formation of 12-coordinate trivalent transuranic MOFs.

To examine the ability of this isorecticular framework to simultaneously incorporate different An(IV), we adopted mixed actinide precursors (Th(IV)-U(IV) and U(IV)-Np(IV), respectively) in equimolar quantities. In the former case, the crystallographically unique An-O bond length and the atomic ratio in leaching supernatant (Figure S13b) collectively indicate that Th(IV) predominates at the 12-coordinate metal center while lower amounts of U(IV) probably reside at defect sites or in the microporous cavities. For the U(IV)-Np(IV) case, it is plausible that U(IV) predominates 12-coordinate metal centers (Table S6). This selectivity for larger An^{4+} among actinide pairs is attributed to the amplification of subtle bonding differences during the crystallization of the high-symmetry framework as well as steric constraints in the accommodation of ADC ligands. Such a selective crystallization pattern is distinct from the conventional selective building of metal-organic complexes^{36,37} and is pivotal to address the challenging intragroup actinide separation. We also probed into the self-assembly mechanism of An-ADC (Figure S14), wherein an appropriate combination of comparatively small θ_1 and θ_2 represents an ingenious arrangement of ligand coordination and configuration meanwhile both strong inter-ligand interactions (Figure S15, Table S5) and the structure-directing role of counteraction for the anionic actinide monomers are involved.

Table 1. Periodic trends of coordinative environment, ligand configuration, and porosity in isorecticular An(IV)-ADC frameworks.

An(IV)-ADC	Th(IV)-ADC	U(IV)-ADC	Np(IV)-ADC	Pu(IV)-ADC
 <p>An-O /Å</p>	2.577(3)	2.532(3)	2.515(4)	2.510(1)
 <p>Bite Angle $\theta_1/^\circ$</p>	50.6	51.3	51.7	51.9
 <p>Twisting Angle $\theta_2/^\circ$</p>	60.7	62.2	61.9	62.1
 <p>Dihedral Angle $\theta_3/^\circ$</p>	120.6	119.4	119.2	119.0
 <p>Dihedral Angle $\theta_4/^\circ$</p>	149.4	150.6	150.8	151.0
 <p>Rectangular pore/Å</p>	7.97 × 5.39	8.01 × 5.22	8.00 × 5.19	8.02 × 5.17
 <p>Accessible void/%</p>	52.0	51.0	50.6	50.4

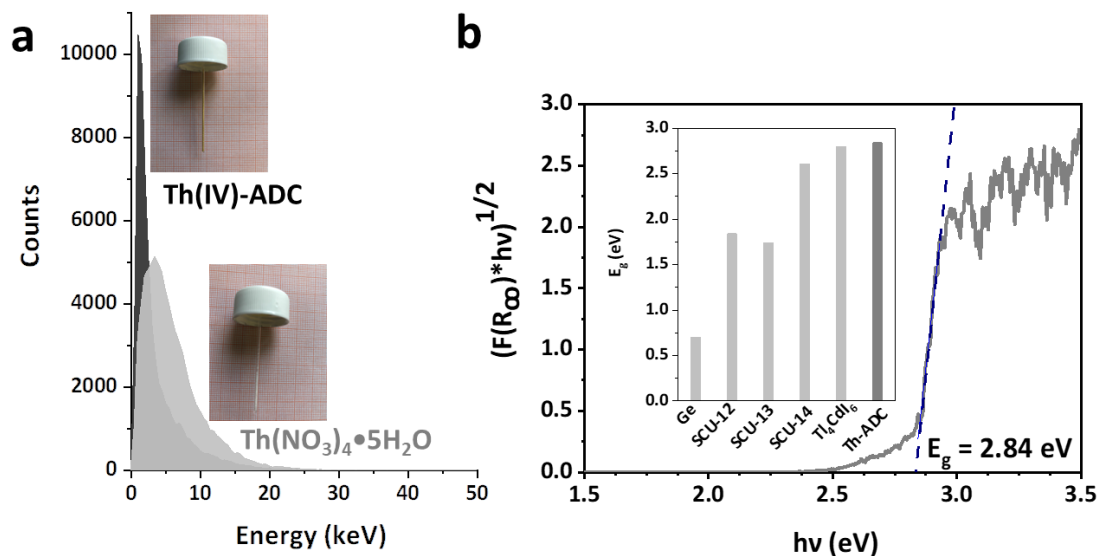


Figure 1. (a) The energy profile of particle detection of Th(IV)-ADC and Th(NO₃)₄•5H₂O. The background count has been subtracted. The inset images are the respective capillaries loaded with pure samples; (b) The UV-Vis DRS of Th(IV)-ADC. The inset histogram is the comparison of the bandgap value of archetypical semiconducting materials for radiation detection.

Anthracene-based MOFs have been well recognized in versatile applications^{38–43}. As crystalline anthracene displays the highest scintillation of any organic scintillator, it is therefore utilized to construct scintillating MOFs as its stability to radiation damage will be improved when incorporated at linker-centric sites⁴⁴ or encapsulated as guest molecules⁴⁵. Th(NO₃)₄•5H₂O yielded 3.29×10^3 counts per second per gram that corresponds to 81% of the ionizing particles emitted by ²³²Th. Th(IV)-ADC exhibited 4.16×10^4 counts per second per gram by producing detectable photons that is an approximately 10-fold enhancement of the autoluminescence (Figure 1a). This increase is lower than that in an autoluminescent MOF⁴⁶, presumably due to its dynamic porosity with non-radiative pathways. As the distances between opposite anthracene planes in Th(IV)-ADC are less than 8.2 Å (Figure S6), an appreciable π -orbital overlap is expected to occur, which facilitates electron transport through anthracene spacing. The strong ionic bonding nature between Th(IV) and carboxylate anions creates a bandgap of 2.84 eV (Figure 1b), which is larger than those in other semiconducting MOFs (i.e. SCU-12⁴⁷, SCU-13⁴⁸, SCU-14⁴⁹), and an iodide-based semiconductor (i.e. Ti₄CdI₆⁵⁰) used for radiation detections. However, its lattices are receptive to vacancies that break up the charge transport pathway and obfuscate intrinsic electroconductivity⁵¹. Th(IV)-ADC can be potentially utilized as a wide-bandgap semiconducting MOF as well as scintillating MOF with constant internal reference for hard radiation detection.

In summary, we have revealed periodic trends in 5f-block metal-oxygen bond length, bite and twisting angle of carboxylate groups, geometry configuration of anthracene plane, and resulting microporosity of isorecticular An(IV)-ADC. The

mixed-valence, mixed-metal issues, and the formation mechanism collectively indicate that this 12-coordinate structure is (1) exclusive to An(IV)-MOFs as a result of a mutual effect of steric hindrance, inter-ligand interactions, and counteraction templating, and (2) conducive to implementing selective crystallization for actinide separation. Quantum chemical calculations reveal that this unusually high CN can only be realized in the high-symmetry environment provided by An(IV)-ADC. The integration of high stability, dynamic porosity, autoluminescence, and semiconductivity confers 12-coordinate An-ADC with potential functionalities such as in-situ identification of airborne isotopes. Future investigations will explore these functionalities and endeavor to expand this actinide structure with CN 12 to An(III) as well as nitrogen analogs of An-ADC.

ASSOCIATED CONTENT

Supporting Information Detailed information on synthesis, characterization, and theoretical calculations.

AUTHOR INFORMATION

Corresponding Author

* Kai Lv

E-mail: lvkai@caep.cn

* Moritz Schmidt

E-mail: moritz.schmidt@hzdr.de

Notes

The authors declare no competing financial interests.

ACKNOWLEDGMENT

This work was supported by the National Natural Science Foundation of China (No.12075214). We also acknowledge Dr. Nina Maria Huittinen for her help in the determination of autoluminescence.

REFERENCES

- Kökçam-Demir, Ü.; Goldman, A.; Esrafilı, L.; Gharib, M.; Morsali, A.; Weingart, O.; Janiak, C. Coordinatively Unsaturated Metal Sites (Open Metal Sites) in Metal-Organic Frameworks: Design and Applications. *Chem. Soc. Rev.* **2020**, *49* (9), 2751–2798. <https://doi.org/10.1039/c9cs00609e>.
- Daly, S. R.; Piccoli, P. M. B.; Schultz, A. J.; Todorova, T. K.; Gagliardi, L.; Girolami, G. S. Synthesis and Properties of a Fifteen-Coordinate Complex: The Thorium Aminodiboranate [Th(H₃BNMe₂BH₃)₄]. *Angew. Chemie - Int. Ed.* **2010**, *49* (19), 3379–3381. <https://doi.org/10.1002/anie.200905797>.
- Kaltsoyannis, N. Seventeen-Coordinate Actinide Helium Complexes. *Angew. Chemie Int. Ed.* **2017**, *56* (25), 7066–7069. <https://doi.org/10.1002/anie.201700245>.
- Yang, L.; Cooper, S.; Kaltsoyannis, N. High Coordination Number Actinide-Noble Gas Complexes; a Computational Study. *Phys. Chem. Chem. Phys.* **2021**, *23* (7), 4167–4177. <https://doi.org/10.1039/D0CP06175A>.
- Ozama, E.; Adachi, S.; Takayanagi, T.; Shiga, M. Quantum Simulation Verifies the Stability of an 18-Coordinate Actinium-Helium Complex. *Chem. Eur. J.* **2018**, *24* (48), 12716–12721. <https://doi.org/10.1002/chem.201802554>.
- Joshi, M.; Ghanty, T. K. Predicted M(H₂)_{12n+} (M = Ac, Th, Pa, U, La and n = 3, 4) Complexes with Twenty-Four Hydrogen Atoms Bound to the Metal Ion. *Chem. Commun.* **2019**, *55* (54), 7788–7791. <https://doi.org/10.1039/C9CC02458A>.
- Hu, S.-X.; Zhang, P.; Zou, W.; Zhang, P. New Theoretical Insights into High-Coordination-Number Complexes in Actinides-Centered Borane. *Nanoscale* **2020**, *12* (28), 15054–15065. <https://doi.org/10.1039/D0NR01955K>.
- Popov, I. A.; Jian, T.; Lopez, G. V.; Boldyrev, A. I.; Wang, L.-S. Cobalt-Centred Boron Molecular Drums with the Highest Coordination Number in the CoB₁₆-Cluster. *Nat. Commun.* **2015**, *6* (1), 8654. <https://doi.org/10.1038/ncomms9654>.
- Li, H.-R.; Liu, H.; Lu, X.-Q.; Zan, W.-Y.; Tian, X.-X.; Lu, H.-G.; Wu, Y.-B.; Mu, Y.-W.; Li, S.-D. Cage-like Ta@Bqn Complexes (n = 23–28, q = -1+3) in 18-Electron Configurations with the Highest Coordination Number of Twenty-Eight. *Nanoscale* **2018**, *10* (16), 7451–7456. <https://doi.org/10.1039/C8NR01087K>.
- Spirlet, M. R.; Rebizant, J.; Apostolidis, C.; Kanellakopoulos, B.; Dornberger, E. Structure of Bis(Ammonium) Hexanitratoplutonium(IV) and Bis(Ammonium) Hexanitratothorium(V). *Acta Crystallogr. Sect. C Cryst. Struct. Commun.* **1992**, *48* (7), 1161–1164. <https://doi.org/10.1107/s0108270191006753>.
- Takao, K.; März, J.; Matsuoka, M.; Mashita, T.; Kazama, H.; Tsushima, S. Crystallization of Colourless Hexanitratoneptunate(IV) with Anhydrous H⁺ Counterions Trapped in a Hydrogen Bonded Polymer with Diamide Linkers. *RSC Adv.* **2020**, *10* (10), 6082–6087. <https://doi.org/10.1039/C9RA10090C>.
- Bowen, S. M.; Duesler, E. N.; Paine, R. T. Synthesis and Crystal and Molecular Structure of a [Diethyl (N,N-Diethylcarbonyl)methylphosphonate]Thorium Nitrate Complex. *Inorg. Chem.* **1982**, *21* (1), 261–265. <https://doi.org/10.1021/ic00131a048>.
- Morse, P. T.; Staples, R. J.; Biros, S. M. Th(IV) Complexes with Cis-Ethylenebis(Diphenylphosphine Oxide): X-Ray Structures and NMR Solution Studies. *Polyhedron* **2016**, *114*, 2–12. <https://doi.org/10.1016/j.poly.2015.05.016>.
- Wang, S.; Alekseev, E. V.; Diwu, J.; Casey, W. H.; Phillips, B. L.; Depmeier, W.; Albrecht-Schmitt, T. E. NDTB-1: A Supertetrahedral Cationic Framework That Removes TeO₄ from Solution. *Angew. Chemie Int. Ed.* **2010**, *49* (6), 1057–1060. <https://doi.org/10.1002/anie.200906397>.
- Kelley, S. P.; Smetana, V.; Emerson, S. D.; Mudring, A.-V.; Rogers, R. D. Benchtop Access to Anhydrous Actinide N-Donor Coordination Complexes Using Ionic Liquids. *Chem. Commun.* **2020**, *56* (30), 4232–4235. <https://doi.org/10.1039/C9CC09852F>.
- Li, Y.; Weng, Z.; Wang, Y.; Chen, L.; Sheng, D.; Diwu, J.; Chai, Z.; Albrecht-Schmitt, T. E.; Wang, S. Surprising Coordination for Low-Valent Actinides Resembling Uranyl(VI) in Thorium(IV) Organic Hybrid Layered and Framework Structures Based on a Graphene-like (6,3) Sheet Topology. *Dalt. Trans.* **2016**, *45* (3), 918–921. <https://doi.org/10.1039/C5DT04183J>.
- Sun, L. J.; Fan, Y. L.; Yin, M. J.; Zhang, H. P.; Feng, H.; Guo, L. J.; Luo, F. Thorium Metal-Organic Framework Showing Proton Transformation from [NH₂(CH₃)₂]+ to the Carboxyl Group to Enhance Porosity for Selective Adsorption of D₂ over H₂ and Ammonia Capture. *Cryst. Growth Des.* **2020**, *20* (6), 3605–3610. <https://doi.org/10.1021/acs.cgd.0c00388>.
- Falaise, C.; Charles, J.-S.; Volklinger, C.; Loiseau, T. Thorium Terephthalates Coordination Polymers Synthesized in Solvothermal DMF/H₂O System. *Inorg. Chem.* **2015**, *54* (5), 2235–2242. <https://doi.org/10.1021/ic502725y>.
- Wang, Y.; Liu, W.; Bai, Z.; Zheng, T.; Silver, M. A.; Li, Y.; Wang, Y.; Wang, X.; Diwu, J.; Chai, Z.; Wang, S. Employing an Unsaturated Th⁴⁺ Site in a Porous Thorium-Organic Framework for Kr/Xe Uptake and Separation. *Angew. Chemie* **2018**, *130* (20), 5885–5889. <https://doi.org/10.1002/ange.201802173>.
- Li, Y.; Weng, Z.; Wang, Y.; Chen, L.; Sheng, D.; Liu, Y.; Diwu, J.; Chai, Z.; Albrecht-Schmitt, T. E.; Wang, S. Centrosymmetric and Chiral Porous Thorium Organic Frameworks Exhibiting Uncommon Thorium Coordination Environments. *Dalt. Trans.* **2015**, *44* (48), 20867–20873. <https://doi.org/10.1039/c5dt03363b>.
- Martin, N. P.; Volklinger, C.; Falaise, C.; Henry, N.; Loiseau, T. Synthesis and Crystal Structure Characterization of Thorium Trimesate Coordination Polymers. *Cryst. Growth Des.* **2016**, *16* (3), 1667–1678. <https://doi.org/10.1021/acs.cgd.5b01746>.
- Li, Y.; Yang, Z.; Wang, Y.; Bai, Z.; Zheng, T.; Dai, X.; Liu, S.; Gui, D.; Liu, W.; Chen, M.; Chen, L.; Diwu, J.; Zhu, L.; Zhou, R.; Chai, Z.; Albrecht-Schmitt, T. E.; Wang, S. A Mesoporous Cationic Thorium-Organic Framework That Rapidly Traps Anionic Persistent Organic Pollutants. *Nat. Commun.* **2017**, *8* (1), 1–10. <https://doi.org/10.1038/s41467-017-01208-w>.
- Falaise, C.; Assen, A.; Mihalcea, T. E.; Volklinger, C.; Mesbah, A.; Dacheux, N.; Loiseau, T. Coordination Polymers of Uranium (IV) Terephthalates. *Dalt. Trans.* **2015**, *44* (6), 2639–2649. <https://doi.org/10.1039/C4DT02343A>.
- Refn, V. E.; Kubus, M.; Mossin, S.; Larsen, R. W.; Pedersen, K. S. A Redox-Innocent Uranium(IV)-Quinoid Metal-Organic Framework. *ACS Omega* **2020**, *5* (7), 3462–3466. <https://doi.org/10.1021/acsomega.9b03727>.
- Lv, K.; Fichter, S.; Gu, M.; März, J.; Schmidt, M. An Updated Status and Trends in Actinide Metal-Organic Frameworks (An-MOFs): From Synthesis to Application. *Coord. Chem. Rev.* **2021**, *446*, 214011. <https://doi.org/10.1016/j.ccr.2021.214011>.
- Gagné, O. C. Bond-Length Distributions for Ions Bonded to Oxygen: Results for the Lanthanides and Actinides and Discussion of the f-Block Contraction. *Acta Crystallogr. Sect. B Struct. Sci. Cryst. Eng. Mater.* **2018**, *74* (1), 49–62. <https://doi.org/10.1107/S2052520617017425>.
- Crawford, M.-J.; Ellern, A.; Karaghiosoff, K.; Mayer, P. Nitrate and Perchlorate Complexes of Uranium(IV). *Inorg. Chem.* **2009**, *48* (23), 10877–10879. <https://doi.org/10.1021/ic901386y>.
- Reilly, S. D.; Scott, B. L.; Gaunt, A. J. [N(n-Bu)₄]₂[Pu(NO₃)₆] and [N(n-Bu)₄]₂[PuCl₆]: Starting Materials To Facilitate Nonaqueous Plutonium(IV) Chemistry. *Inorg. Chem.* **2012**, *51* (17), 9165–9167. <https://doi.org/10.1021/ic301518g>.
- Shannon, R. D. Revised Effective Ionic Radii and Systematic Studies of Interatomic Distances in Halides and Chalcogenides. *Acta Crystallogr. Sect. A* **1976**, *32* (5), 751–767. <https://doi.org/10.1107/S0567739476001551>.
- Hastings, A. M.; Ray, D.; Jeong, W.; Gagliardi, L.; Farha, O. K.; Hixon, A. E. Advancement of Actinide Metal-Organic Framework Chemistry via Synthesis of Pu-UiO-66. *J. Am. Chem. Soc.* **2020**, *142* (20), 9363–9371. <https://doi.org/10.1021/jacs.0c01895>.

- (31) Sykora, R. E.; Assefa, Z.; Haire, R. G.; Albrecht-Schmitt, T. E. Synthesis, Structure, and Spectroscopic Properties of Am(III) and the Photoluminescence Behavior of Cm(III). *Inorg. Chem.* **2005**, *44* (16), 5667–5676. <https://doi.org/10.1021/ic050386k>.
- (32) Ridenour, J. A.; Surbella, R. G.; Gelis, A. V.; Koury, D.; Poineau, F.; Czerwinski, K. R.; Cahill, C. L. An Americium-Containing Metal–Organic Framework: A Platform for Studying Transplutonium Elements. *Angew. Chemie Int. Ed.* **2019**, *58* (46), 16508–16511. <https://doi.org/10.1002/anie.201909988>.
- (33) Chesman, A. S. R.; Yang, M.; Mallick, B.; Ross, T. M.; Gass, I. A.; Deacon, G. B.; Batten, S. R.; Mudring, A.-V. Melting Point Suppression in New Lanthanoid(III) Ionic Liquids by Trapping of Kinetic Polymorphs: An in Situ Synchrotron Powder Diffraction Study. *Chem. Commun.* **2012**, *48* (1), 124–126. <https://doi.org/10.1039/C1CC14744G>.
- (34) Yang, X.-F.; Ren, P.; Yang, Q.; Geng, J.-S.; Zhang, J.-Y.; Yuan, L.-Y.; Tang, H.-B.; Chai, Z.-F.; Shi, W.-Q. Strong Periodic Tendency of Trivalent Lanthanides Coordinated with a Phenanthroline-Based Ligand: Cascade Countercurrent Extraction, Spectroscopy, and Crystallography. *Inorg. Chem.* **2021**, *60* (13), 9745–9756. <https://doi.org/10.1021/acs.inorgchem.1c01035>.
- (35) Barnard, R.; Bullock, J. I.; Gellatly, B. J.; Larkworthy, L. F. Chemistry of the Trivalent Actinides. Part III. Some Chemical and Physical Properties of Hydrated Uranium(III) Fluoride and the Anhydrous Chloride, Bromide, and Iodide. The Stability of Uranium(III) in Aqueous Solution and in Organic Solvents. *J. Chem. Soc. Dalton Trans.* **1973**, No. 6, 604. <https://doi.org/10.1039/dt9730000604>.
- (36) Li, X.-Z.; Zhou, L.-P.; Yan, L.-L.; Dong, Y.-M.; Bai, Z.-L.; Sun, X.-Q.; Diwu, J.; Wang, S.; Bünzli, J.-C.; Sun, Q.-F. A Supramolecular Lanthanide Separation Approach Based on Multivalent Cooperative Enhancement of Metal Ion Selectivity. *Nat. Commun.* **2018**, *9* (1), 547. <https://doi.org/10.1038/s41467-018-02940-7>.
- (37) Mei, L.; Ren, P.; Wu, Q.; Ke, Y.; Geng, J.; Liu, K.; Xing, X.; Huang, Z.; Hu, K.; Liu, Y.; Yuan, L.; Mo, G.; Wu, Z.; Gibson, J. K.; Chai, Z.; Shi, W. Actinide Separation Inspired by Self-Assembled Metal–Polyphenolic Nanocages. *J. Am. Chem. Soc.* **2020**, *142* (39), 16538–16545. <https://doi.org/10.1021/jacs.0c08048>.
- (38) Liu, X.; Liu, B.; Li, G.; Liu, Y. Two Anthracene-Based Metal–Organic Frameworks for Highly Effective Photodegradation and Luminescent Detection in Water. *J. Mater. Chem. A* **2018**, *6* (35), 17177–17185. <https://doi.org/10.1039/C8TA03807D>.
- (39) Wang, C.; Volotskova, O.; Lu, K.; Ahmad, M.; Sun, C.; Xing, L.; Lin, W. Synergistic Assembly of Heavy Metal Clusters and Luminescent Organic Bridging Ligands in Metal–Organic Frameworks for Highly Efficient X-Ray Scintillation. *J. Am. Chem. Soc.* **2014**, *136* (17), 6171–6174. <https://doi.org/10.1021/ja500671h>.
- (40) Rowe, J. M.; Zhu, J.; Soderstrom, E. M.; Xu, W.; Yakovenko, A.; Morris, A. J. Sensitized Photon Upconversion in Anthracene-Based Zirconium Metal–Organic Frameworks. *Chem. Commun.* **2018**, *54* (56), 7798–7801. <https://doi.org/10.1039/C8CC01893F>.
- (41) Ghalei, B.; Wakimoto, K.; Wu, C. Y.; Isfahani, A. P.; Yamamoto, T.; Sakurai, K.; Higuchi, M.; Chang, B. K.; Kitagawa, S.; Sivaniah, E. Rational Tuning of Zirconium Metal–Organic Framework Membranes for Hydrogen Purification. *Angew. Chemie Int. Ed.* **2019**, *58* (52), 19034–19040. <https://doi.org/10.1002/anie.201911359>.
- (42) Roy, S.; Mostakim, S.; Barman, S.; Paul, S.; De, R.; Reinsch, H.; Grzywa, M.; Stock, N.; Volkmer, D.; Biswas, S. An Anthracene-Based Metal–Organic Framework for Selective Photo-Reduction of Carbon Dioxide to Formic Acid Coupled with Water Oxidation. *Chem. Eur. J.* **2020**, chem.202004596. <https://doi.org/10.1002/chem.202004596>.
- (43) Chen, D.; Xing, H.; Su, Z.; Wang, C. Electrical Conductivity and Electroluminescence of a New Anthracene-Based Metal–Organic Framework with π -Conjugated Zigzag Chains. *Chem. Commun.* **2016**, *52* (10), 2019–2022. <https://doi.org/10.1039/C5CC09065B>.
- (44) Doty, F. P.; Bauer, C. A.; Skulan, A. J.; Grant, P. G.; Allendorf, M. D. Scintillating Metal–Organic Frameworks: A New Class of Radiation Detection Materials. *Adv. Mater.* **2009**, *21* (1), 95–101. <https://doi.org/10.1002/adma.200801753>.
- (45) Boudjema, L.; Toquer, G.; Basta, A. H.; Trens, P.; Lerner, D. A. Confinement-Induced Electronic Excitation Limitation of Anthracene: The Restriction of Intramolecular Vibrations. *J. Phys. Chem. C* **2018**, *122* (49), 28416–28422. <https://doi.org/10.1021/acs.jpcc.8b09904>.
- (46) Andreo, J.; Priola, E.; Alberto, G.; Benzi, P.; Marabello, D.; Proserpio, D. M.; Lamberti, C.; Diana, E. Autoluminescent Metal–Organic Frameworks (MOFs): Self-Photoemission of a Highly Stable Thorium MOF. *J. Am. Chem. Soc.* **2018**, *140* (43), 14144–14149. <https://doi.org/10.1021/jacs.8b07113>.
- (47) Wang, Y.; Liu, X.; Li, X.; Zhai, F.; Yan, S.; Liu, N.; Chai, Z.; Xu, Y.; Ouyang, X.; Wang, S. Direct Radiation Detection by a Semiconductive Metal–Organic Framework. *J. Am. Chem. Soc.* **2019**, *141* (20), 8030–8034. <https://doi.org/10.1021/jacs.9b01270>.
- (48) Liang, C.; Zhang, S.; Cheng, L.; Xie, J.; Zhai, F.; He, Y.; Wang, Y.; Chai, Z.; Wang, S. Thermoplastic Membranes Incorporating Semiconductive Metal–Organic Frameworks: An Advance on Flexible X-ray Detectors. *Angew. Chemie Int. Ed.* **2020**, *59* (29), 11856–11860. <https://doi.org/10.1002/anie.202004006>.
- (49) Cheng, L.; Liang, C.; Liu, W.; Wang, Y.; Chen, B.; Zhang, H.; Wang, Y.; Chai, Z.; Wang, S. Three-Dimensional Polycatenation of a Uranium-Based Metal–Organic Cage: Structural Complexity and Radiation Detection. *J. Am. Chem. Soc.* **2020**, *142* (38), 16218–16222. <https://doi.org/10.1021/jacs.0c08117>.
- (50) Wang, S.; Liu, Z.; Peters, J. A.; Sebastian, M.; Nguyen, S. L.; Malliakas, C. D.; Stoumpos, C. C.; Im, J.; Freeman, A. J.; Wessels, B. W.; Kanatzidis, M. G. Crystal Growth of Ti4CdI6: A Wide Band Gap Semiconductor for Hard Radiation Detection. *Cryst. Growth Des.* **2014**, *14* (5), 2401–2410. <https://doi.org/10.1021/cg5001446>.
- (51) Xie, L. S.; Skorupskii, G.; Dincă, M. Electrically Conductive Metal–Organic Frameworks. *Chem. Rev.* **2020**, *120* (16), 8536–8580. <https://doi.org/10.1021/acs.chemrev.9b00766>.

For Table of Contents Only

